Cocrystallization of curcumin with benzenediols and benzenetriols via rapid solvent removal

Si Nga Wong[1,#], Shenye Hu[2,#], Wai Wing Ng[3], Xiaoyan Xu[1], Ka Lun Lai[3], Wai Yip Thomas Lee[4], Albert Hee Lum Chow[3], Changquan Calvin Sun[2,*], Shing Fung Chow[1,*]

[1]Department of Pharmacology and Pharmacy, Li Ka Shing Faculty of Medicine, The University of Hong Kong, Pokfulam, Hong Kong

[2]Pharmaceutical Materials Science and Engineering Laboratory, Department of Pharmaceutics, College of Pharmacy, University of Minnesota, USA

[3]School of Pharmacy, The Chinese University of Hong Kong, Sha Tin, Hong Kong

[4]Aptorum Therapeutics Limited, Unit 232, 12 Science Park W Ave, Shatin, Hong Kong

# *Equal contribution

* *Corresponding authors*

Changquan Calvin Sun
Department of Pharmaceutics
College of Pharmacy
University of Minnesota
9-127B Weaver Densford Hall
308 Harvard Street S.E.
Email: sunx0053@umn.edu
Tel: +1-612-624-3722
Fax: +1-612-626-2125

Shing Fung Chow
Department of Pharmacology and Pharmacy
Li Ka Shing Faculty of Medicine
The University of Hong Kong
L2-08B, Laboratory Block,
21 Sassoon Road, Pokfulam, Hong Kong
Email: asfchow@hku.hk
Tel: +852-39179026
Fax: +852-28170859

ABSTRACT

Recent advance in crystal engineering by cocrystallization has offered a promising approach for tackling undesirable physicochemical properties of drug substances. In this study, various structurally similar benezenediols and benezenetriols, namely catechol (CAT), resorcinol (RES), hydroquinone (HYQ), hydroxyquinol (HXQ) and pyrogallol (PYR), were employed as coformers to obtain phase pure cocrystals with curcumin (CUR) by rapid solvent evaporation of solutions. We successfully prepared two new cocrystals, CUR-CAT and CUR-HYQ, and a new polymorph of cocrystal CUR-HXQ. Both could not be obtained by traditional cocrystallization methods. Their 1:1 stoichiometry was confirmed by the construction of binary phase diagram through differential scanning calorimetry (DSC) analysis. The hygroscopicity, dissolution, and tableting performance of the resulting cocrystals were evaluated. Compared to the individual constituent coformers, cocrystals exhibited profound improvement in the stability against high humidity. The CUR-HXQ cocrystal displayed 7 times faster intrinsic dissolution rate than CUR. Four out of the five cocrystals had better tabletability. This work demonstrated the effectiveness of discovering cocrystals by kinetic entrapment using fast solvent removal approach. Some of these cocrystals possess improved pharmaceutical properties for future development of solid dosage forms of CUR.

Keywords: Cocrystal, Crystal Engineering, Benezenediols, Benezenetriols, Curcumin, Intrinsic Dissolution Rate, Tabletability, Solid-state characterization

1. Introduction

Cocrystallization as a formulation strategy to remedy issues associated with poorly soluble drugs has gained much popularity during the past two decades. Pharmaceutical cocrystals may be defined as homogenous crystalline materials incorporating two or more different molecules, with at least one of them as active pharmaceutical ingredients (APIs), in a definite stoichiometric ratio where the crystal structure is maintained by nonionic and noncovalent bonds, including hydrogen bonds [1-2]. In the context of crystal engineering, cocrystallization represents a promising alternative to the formation of solvates/hydrates, polymorphs, and salts for modifying the physicochemical properties of the APIs whilst preserving the integrity of their molecular structures. Cocrystallization is a more versatile technology than salt formation because it is applicable to weakly ionizable and neutral compounds of which the proton transfer capability is restricted [3]. Advantages of cocrystals in enhancing the solubility, dissolution performance, hygroscopicity, stability, and tabletability of APIs have been amply shown [4-9]. Both judicious selection of coformers and effective synthesis methods are critical for successful development of pharmaceutical cocrystals.

To date, approximately 3,000 substances are listed in the Everything Added to Food in the United States (EAFUS) list, comprising the Generally Regarded as Safe (GRAS) ingredients and safe food additives. They can be employed as potential coformers for the cocrystal preparation [9]. Cocrystallization not only offers new opportunities in intellectual property [10], but also facilitates the development of combination therapies (e.g., drug-drug, drug-herb, and herb-herb cocrystals for various diseases) [11-12], and personalized medicines in light of a higher degree of flexibility. By designing the crystal form of a given drug with various coformers in the proper stoichiometric ratios, different drug release profiles (e.g., immediate release and sustained release) [13] may be achieved, which may be utilized to alleviate drug overdosing and adverse reactions [14] to improve patient compliance.

Pharmaceutical cocrystals are conventionally prepared by solid state grinding [15], slow solvent evaporation [16], antisolvent addition [17], slurry conversion [18] and recrystallization from melt [19]. While the trial-and-error screening approach is still the mainstream in cocrystal discovery, the sheer number of possible coformers renders the

tactless screening process time-consuming and costly. New alternative techniques based on supramolecular synthons [20], Hansen solubility parameters [21] and conductor-like screening model for real solvents (COSMO-RS) [22], have emerged. More effective cocrystal screening through structural resemblance, as exemplified by Springuel et al, has also been introduced [23]. In this approach, coformers with similar functional groups are expected to be likely to yield cocrystals with identical APIs owing to the presence of similar intermolecular interactions for assembling multicomponent systems. Thus, studying cocrystallization using structurally similar coformer isomers is a useful approach in probing intermolecular forces responsible to cocrystal formation. However, no one-size-fits-all method is currently available for fabricating all the cocrystal forms of a given API, even with the approach of structurally related coformers. Such incongruity of cocrystal formation ability may be partly attributed to the intriguing interplay between the thermodynamics and kinetics of the cocrystallization process [24]. One cannot exclude the possibility of hidden cocrystals, which have not been readily discovered via standard methods due to their inherent thermodynamically unstable nature. To isolate such metastable cocrystals, kinetic approaches, such as rotary evaporation and spray drying, are desired since the solvent is removed so rapidly that the molecules can crystallize into less stable solid forms and isolated before they have sufficient time to convert to the most stable crystal form [24-25].

Curcumin (CUR), 1,7-bis(4-hydroxy-3-methoxyphenyl)-1,6-heptadiene-3,5-dione, is a natural polyphenolic compound derived from the rhizomes of the herb turmeric (*Curcuma longa* Linn). For centuries, abundant *in vitro* and *in vivo* studies have reported curcumin *per se* exhibits potent anti-oxidant [26], anti-inflammatory [27], anti-microbial [28-29], anti-spasmodic [30], lipid lowering [31], pro-cognitive [32], neuro- and hepato-protective [33-34] properties. As a GRAS compound, CUR is safe even at high dose, i.e., it can be dosed up to 12000 mg/day and its Allowable Daily Intake (ADI) value is 0–3 mg/kg bodyweight [35-37]. Its tremendous pharmacotherapeutic values together with the safety, tolerability, and affordability, have created interest in using CUR for therapeutic interventions against various chronic diseases, including cancers, diabetes, pulmonary, cardiovascular, autoimmune, and neurodegenerative diseases [38]. However, the clinical translation of CUR is severely hindered by its limited systemic bioavailability, due to low solubility (ca. 11

ng/ml), and poor pharmacokinetic profile [39]. Besides, CUR possesses poor compressibility such that no intact tablets could be formed at 50 MPa or higher pressures [24], which presents a challenge for the formulation development and manufacturing. CUR is a pan-assay interference compound, that can undergo tautomerization in solution [40].

To improve the pharmaceutical properties, cocrystals of curcumin with resorcinol and pyrogallol were obtained from solutions mediated by the phenol−carbonyl and phenol−phenol intermolecular hydrogen bonds. However, interestingly, efforts of preparing CUR cocrystals with other structurally related polyphenolics, such as catechol, phloroglucinol, and hydroquinone, had failed via the same preparation method [41]. This may be due to the cocrystal metastability, which may be addressed through entrapping kinetic solid forms using procedures, such as fast solvent removal [24]. Thus, a goal of this study was to investigate the potential of utilizing the kinetic approach, i.e., rotary evaporation, along with the selection of an array of coformers of similar molecular structures as a rational cocrystal screening method to increase the probability of successful cocrystallization of CUR. Five commercially available benzenediol and benzenetriol isomers (Figure 1), catechol (CAT), resorcinol (RES), hydroquinone (HYQ), hydroxyquinol (HXQ), and pyrogallol (PYR) were used as coformers, which differ in the positions and number of hydroxyl groups on the benzene ring.

Many of the chosen phenolic coformers have been reported to possess antioxidant and antimicrobial activities that potentially produce synergistic effects with CUR against various cancers [42-43]. Although not all of them are on the GRAS list, they are valuable for providing a better understanding in the cocrystallization process and outcomes. Systematic analysis of the relationships among chemistry of coformers and pharmaceutical performance of cocrystals may provide insight into the design of new cocrystals exhibiting tailor-made properties.

2. Experimental Section

2.1. Materials

Curcumin (CUR, purity >99.5%) was sourced from Yung Zip Chemical (Taiwan). The coformers, namely catechol (CAT), resorcinol (RES), hydroquinone (HYQ), hydroxyquinol (HXQ) and pyrogallol (PYR), were purchased from Sigma-Aldrich (St.

Louis, MO, USA) and Alfa Aesar (Ward Hill, MA, USA). Acetone of analytical grade was obtained from Merck KGaA (Darmstadt, Germany). Water was purified though a Direct-Q water purifier (Water Corp., Milford, MA) with resistivity not less than 18.0 MΩ-cm. All chemicals and solvents were used as received, except for RES, which was gently grinded to produce a powder for the ease of accurate weighing.

2.2. Preparation of Cocrystals

Equimolar amounts (0.814 mmol) of CUR (300 mg) and cocrystal former (CAT: 89.67 mg, RES: 89.67 mg, HYQ: 89.67 mg, HXQ: 102.7 mg and PYR: 102.7 mg) were dissolved in 100 mL acetone and mixed until a homogenous solution was obtained, for either slow or rapid solvent evaporation. For slow evaporation, the prepared solutions were sealed with a perforated film and dried in fumehood for 72 hours. Rapid solvent removal was performed by a rotary evaporator (Buchi, Germany) under a vacuum with the rotary flask being immersed in a water bath at 40 °C. The resulting product was dried in an oven at 60 °C for 3 hours to remove residual solvent and grinded to a fine powder for further analysis. All samples were stored promptly after drying to avoid photo-degradation and moisture sorption. Multiple batches of cocrystal sample were combined into a single batch (10-15 g) for the intrinsic dissolution rate determination and compaction study.

2.3. Solubility Determination

The solubilities of CUR and coformers in acetone were determined by adding excess solid in screw-capped test tubes with 3 mL of acetone and shaking for 72 hours. Samples filtered through 0.45 μm membrane filters, followed by dilution to appropriate concentrations for HPLC assay (see Section 2.4).

2.4. High Performance Liquid Chromatography (HPLC)

The amounts of CUR and coformers in the solubility study were determined using an Agilent 1200 series HPLC system (Agilent Technologies, USA, equipped with a diode array detector) with an Agilent Zorbax Eclipse Plus C18 column (5 μm, 250 mm× 4.6 mm). The mobile phase consisted of acetonitrile (A) and 0.01% (v/v) aqueous trifluoroacetic acid (B) was run at various v/v ratios (CAT: 30%A and 70%B; RES, HYQ, and PYR: 10%A and 90%B; HXQ: 90%A and 10%B) and absorbance was measured at

appropriate wavelengths (CAT, RES, HYQ, and PYR: 268 nm; HXQ: 292 nm). Injection volume was 10 μL and flow rate was 1 mL/min at room temperature.

2.5. Differential Scanning Calorimetry (DSC)

Thermograms were generated through a differential scanning calorimeter (Q6000, PerkinElmer, Waltham, MA), using nitrogen as a purge gas at a flow rate of 20 mL/min. Calibration for enthalpy and cell constant was conducted with high purity indium prior to the analysis. Accurately weighed samples (3–5 mg) were encapsulated in hermetically sealed aluminum pans with pinhole-vented lid if required and heated from 50 °C to 250 °C at 10 °C/min. Same experimental conditions were applied to the construction of temperature-composition phase diagrams. The Pyris manager software was used for analyzing the data.

2.6. Powder X–Ray Diffraction (PXRD)

A Panalytical X-ray diffractometer (Philips X'Pert PRO, The Netherlands), operated with Cu-Kα radiation (lambda= 1.5406 Å, 40kV, 40mA), was used to collect the X-ray powder diffraction data. Sample was evenly packed in an aluminum holder with a 2 mm depth and scanned from 2θ interval of 2° to 40° at 0.05° step size with 4° per minute scanning speed.

2.7. Fourier-Transform Infrared (FTIR) Spectroscopy

The FTIR spectra were obtained with a FTIR spectrophotometer (SpectrumBX, Perkin Elmer, Waltham, MA) in KBr diffuse reflectance mode. The scan was performed in the range of 4,000 cm^{-1} to 600 cm^{-1} at an interval of 0.5 cm^{-1}. A total of 64 scans were collected at a resolution of 4 cm^{-1} for each sample.

2.8. Intrinsic Dissolution Rate Measurement

Intrinsic dissolution rate (IDR) was measured using the rotating disc method. Powder of about 15mg was compressed at 1000 lb force and held for 2min, using a custom-made stainless-steel die (6.39 mm in diameter) against a flat stainless-steel disc, to prepare pellet with a visually smooth exposed surface that was coplanar with the surface of the die. While rotating at 300 rpm, the die was immersed in 500 mL of the dissolution medium at 25 ^{o}C. Because CUR has an extremely low aqueous solubility, the IDR study was conducted using isopropyl alcohol instead of pure water as the dissolution

medium. UV absorbance of the solution was continuously monitored using a UV−vis fiber optic probe (Ocean Optics, Dunedin, FL) connected to a computer. Absorbance data were converted into concentrations using a calibration curve, constructed using the same setup, to obtain concentration−time profiles. Finally, IDR was calculated from the slope of an appropriate linear portion of the dissolution curve and the total pellet surface area exposed to the dissolution medium.

2.9. Dynamic Vapor Sorption (DVS)

Water sorption-desorption isotherms were obtained using an automated moisture balance (Intrinsic DVS, Surface Measurement Systems Ltd., Allentown, PA, USA) at 25 ^{o}C. The nitrogen flow rate was 50 mL/min. During a routine analysis, a sample was equilibrated at each step with the equilibration criteria of either dm/dt <0.003% or maximum equilibration time of 6 h. Once one of the criteria was met, the relative humidity (RH) was changed to the next target value following a 0% – 95% – 0% RH cycle with a step size of 5%.

2.10. Powder Compaction Analysis

All powders were gently grinded to minimize the variation in particle size [44] and/or morphology [45] among samples. Similarity in particle size and shape was verified using a polarized light microscope before the compaction analysis. Approximately 200 mg of powder was manually filled into an 8 mm diameter flat-faced tableting die and a universal material testing machine (model 1485; Zwick/Roell, Ulm, Germany) was used to compress the powders at a speed of 5 mm/min. Tablets were allowed to relax under ambient environment for 24 h before measuring their diameters, thicknesses, and weights. Care was taken to remove flashing before measuring tablet thickness [46]. Their diametrical breaking forces were then measured using a texture analyzer (TA-XT2i; Texture Technologies Corporation, Scarsdale, New York) at the speed of 0.01 mm/s. Tablet tensile strength was calculated from the maximum breaking force and tablet dimensions following the standard procedure [47]:

$$\sigma = \frac{2F}{10^6 \pi D T}$$

where σ is tensile strength (MPa), *F* is the breaking force (N), *D* is the tablet diameter (m), and *T* is the thickness of tablet (m). Tabletability profiles were generated by plotting tensile strength as a function of compaction pressure.

3. Results and Discussion

3.1. Cocrystallization of Curcumin with Benzenediols and Benzenetriols

CUR could cocrystalize with RES, PYR, and HXQ [41, 48]. However, previous attempts to prepare CUR cocrystals with structurally similar coformers, including CAT, PHL, and HYQ, by means of slow solvent evaporation or liquid-assisted grinding were unsuccessful [41]. CUR-HYQ (1:1) could only form a binary eutectic via mechano-chemical grinding [49]. However, rapid solvent removal by rotary evaporation was used to successfully prepare the kinetically stable CUR-PHL cocrystal [24]. Here, we further tested the ability of such method for preparing phase pure curcumin cocrystals with the five benezendiols and benezentriols, namely CAT, RES, HYQ, HXQ, and PYR.

Cocrystals with all five coformers were successfully obtained in 1:1 stoichiometric ratio from acetone. The PXRD patterns of the prepared samples exhibited a number of distinct diffraction peaks while characteristic peaks corresponding to CUR and coformers were absent (Figure 2). The XRD patterns of CUR-RES (2θ = 10.68°, 10.86°, 11.8°, 12.83° and 18.82°) and CUR-PYR (2θ = 10.35°, 10.86°, 11.76° and 18.65°) were in concordance with the reported results using simple solution crystallization [41], while those of CUR-HXQ (2θ = 5.7°, 6.03°, 9.69°, 10.12°, 12.1°, 13.06° and 18.04°) were explicitly different from that prepared through melt crystallization [48]. Therefore, polymorphism of CUR-HXQ is indicated, which may be attributed to different experimental conditions employed that influenced the processes of nucleation and crystal growth [50]. In addition, the diffraction pattern of CUR-HXQ reported in the literature exhibited relatively low crystallinity compared to the one illustrated in this study (Figure 2d). For the CUR-HYQ and CUR-CAT systems, the characteristic diffraction peaks of cocrystal formers and new phases were identified as follows: CUR 2θ = 7.95°, 8.9° and 17.25°; HYQ 2θ = 4.61°; CAT 2θ =10.09°, 16.36° and 20.12°; CUR-HYQ 2θ = 10.57°, 11.51°, 13.21°, 18.34°; CUR-CAT 2θ = 9.03°, 10.58°, 10.95°, 11.87° and 18.77°. The

absence of characteristic peaks of CUR and corresponding cocrystal formers confirmed the high purity of the cocrystal samples prepared. Interestingly, some of the diffraction peaks are shared among all the resulting cocrystals. For example, a duplet appeared in the range of 2θ at around 10.5° and 11.8° was commonly observed (as denoted by * in Figure 2). Similar peaks were observed for CUR-HXQ but have shifted to higher angles, i.e., 2θ = ~12.1° and 13°. The presence of peaks at similar low 2 theta angles in PXRD suggests similar molecular layers with large d-spacing in these cocrystals.

To ensure the successful solvent-mediated cocrystallization of CUR, the choice of solvent is critical for determining the tautomeric equilibrium of CUR in solution and the relative solubility of the cocrystal formers, since they affect the propensity of formation and phase purity of cocrystal [24]. In view of the structural resemblance of the chosen coformers to PHL, acetone was deemed appropriate as the crystallization solvent for the preparation of other CUR-benzenediol/benzenetriol cocrystals. This is because of the similar interactions with acetone in these cocrystal systems to the CUR-PHL system. Ideally, the solubility of two cocrystal formers in the solvent should be congruent in order to prevent the precipitation of the less soluble CUR from solution prematurely prior to reaching the labile zone for spontaneous cocrystallization. This explains the failure of generating the metastable CUR cocrystals using slow solvent evaporation in acetone (Figure S1) because CUR and the polyphenolic coformers exhibit incongruent solubility (Table S1).

Here, rapid solvent evaporation was again a prerequisite for successfully preparing elusive CUR-CAT, CUR-HYQ, and CUR-HXQ cocrystals. The effectiveness of this technique arises from important role of kinetics in the process of crystallization as stated by the Ostwald's rule of successive stages, where the metastable form appears in the early stage of crystallization, followed by phase transformation to the most stable form in order to reach the equilibrium [24, 51]. Thus, the crystallization of cocrystals under a rapid crystallization rate and high degree of supersaturation conditions favored the nucleation of kinetically stable cocrystals, which effectively overcome the problem due to the incongruent solubilities of the two coformers [24].

3.2. Thermal Properties and Stability

The melting points of CUR-RES (171.2 °C) and CUR-HXQ (165.0 °C) measured by DSC (Figure 3) are consistent with those reported in literature [41, 48]. However, the melting point of CUR-PYR (165.7 °C) in this work is approximately 10 °C higher than that reported by Sanphui et al [41]. Based on the PXRD result, the higher melting point of CUR-PYR should not be due to polymorphism but probably a higher phase purity of our raw CUR, reflected by the higher melting point of our CUR. For the CUR-HXQ system, the presence of a small endothermic event at 128.8 °C in the DSC thermogram may be attributed to polymorphic phase transition if the two polymorphs are enantiotropically related according to the heat of transition rule [52]. With regards to the newly discovered CUR-HYQ and CUR-CAT cocrystals, the DSC thermograms show sharp single melting endotherm with peaks at 157.9 °C and 152.0 °C, respectively (Figure 3a, 3c), indicative of homogenous solid phase with high phase purity. The enthalpy of fusion (ΔH_f) of all cocrystal systems (CUR-CAT: 72 kJ/mol; CUR-RES: 63.8 kJ/mol; CUR-HYQ: 51.7 kJ/mol; CUR-HXQ: 73.9 kJ/mol; CUR-PYR: 60.3 kJ/mol) are significantly higher than their starting materials (Table 1), suggesting the crystal lattice strengthening upon cocrystallization. On the basis of PXRD patterns, no phase transformation was observed and all of the cocrystals remained stable at the stressed condition at 60 °C for 1 month when kept dry (Figure S2).

It is worth noting that, as with the CUR-RES, CUR-PYR and CUR-HXQ systems, the melting point of CUR-CAT lies between that of the starting materials, i.e., CUR (183.2 °C) and CAT (104.9 °C). However, similar to the previously reported CUR-PHL system, the melting point of CUR-HYQ is lower than that of CUR and HYQ (173.0 °C). This, along with the lower enthalpy of fusion (Table 1), suggests weaker intermolecular interactions in CUR-PHL and CUR-HYQ than other CUR cocrystals. This is consistent with the metastable nature of these two systems, which is responsible to the elusiveness in the previous effort to prepare them by slow evaporation.

To further assess the new phase, temperature-composition phase diagrams were constructed using binary mixtures of cocrystal formers with mole fractions ranging from 0 to 1, through DSC analysis (Figure 4). The solidus temperatures, shown in square, represent the onset temperatures of the first endotherms while the liquidus temperatures,

shown in diamond, are the peak temperatures of the second endotherms. Binary phase diagram construction using thermal analysis has been traditionally applied in characterizing solid solution and eutectic mixture for a given system. It has been adopted for conducting efficient and comprehensive cocrystal screening [53-54]. The phase diagram for each of the cocrystal systems in this study revealed a congruent melting temperature at 50% molar composition of either cocrystal former, which indicates a 1:1 stoichiometry. Each of them also displayed two eutectics (Table 1), with compositions lying between cocrystal and CUR, and between cocrystal and coformer, respectively. It was reported that CUR-HXQ cocrystal could be formed using mixtures containing CUR at mole fractions of 0.33 via melt crystallization [48]. However, no signs of the 1:2 CUR-HXQ cocrystal was observed in this study (Figure 4d). It is possible that the reported 1:2 CUR-HXQ cocrystal [48] may correspond to a eutectic, not a cocrystal.

The eutectic melting temperature is 137.5 °C for CUR and HYQ [49]. As described by Yamashita et al., three characteristic DSC peaks, corresponding to the thermal events of starting materials melting, cocrystal formation and cocrystal melting, should be observed in the DSC diagram for physical mixture capable of cocrystal formation [55]. That is, CUR and HYQ should melt at 137.5 °C, recrystallize into CUR-HYQ cocrystal, which melts at 157.9 °C again. Such phenomenon was observed in the previous study aimed at preparing this cocrystal whereas absent in our study. The chance of cocrystal melting being shadowed by other events is minimal, as the melting point of the cocrystal (157.9 ^{o}C) is 20°C higher than the eutectic melting temperature. The failure of the previous efforts in preparing the CUR-HYQ cocrystals highlights the importance of kinetic control in preparing metastable solid forms, including metastable cocrystals. We have found that the use of suitable solvent and fast solvent removal using rotary evaporation are both pivotal to the success in CUR-HYQ and CUR-PHL metastable cocrystal preparation. Although mechanical grinding can be beneficial to thermodynamically stable cocrystal systems with the merits of low processing cost and high efficiency, it also presents the risk of missing metastable cocrystals. However, cocrystals, which were predicted to exist based on structural resemblance of coformers but failed to be experimentally confirmed, may be prepared using the rapid solvent removal method.

3.3. FTIR Spectroscopic Analysis

Compared to their corresponding starting materials, FTIR spectral peak shifts for various functional groups have been observed in the cocrystals (Figure 5 and Table 2), suggesting the alteration of molecular environment around these groups in the solid state. The major absorption peaks of CUR-RES and CUR-PYR are comparable to those in literature [41]. However, a ~15-unit deviation has been observed in the phenolic O-H stretching of CUR-HXQ as compared with the reported data [48]. This may be, again, attributed to the polymorphism of this cocrystal. CUR-HYQ and CUR-CAT exhibited broad and prominent absorption peaks between 3200 and 3700 cm^{-1}, which correspond to phenolic O-H stretching (CUR-HYQ: 3432 cm^{-1}; CUR-CAT: 3409 and 3449 cm^{-1}). The dramatic decrease in wavelength of phenolic O-H stretching from 3506 cm^{-1} (CUR) to a lower frequency implies the involvement of the O-H group in a strong intermolecular hydrogen bond without proton transfer, confirming the formation of new phases. The extent of phenolic O-H shift is more significant in CUR-benezenetriol cocrystals (CUR-HXQ: 3423 cm^{-1}; CUR-PHL: 3412 cm^{-1}; CUR-PYR: 3401 cm^{-1}) than those observed in CUR-benezenediol cocrystals (CUR-CAT: 3449 and 3409 cm^{-1}; CUR-RES: 3437 cm^{-1}; CUR-HYQ: 3432 cm^{-1}). This can be ascribed to the structural differences among coformer molecules, in which benezenetriols contain an additional hydroxyl group for participation in hydrogen bond formation. Additionally, no spectral shift for C=O stretching was evident in all cocrystals. This suggests the inactive role of carbonyl groups in the intermolecular interactions, e.g., hydrogen bonding, in these cocrystals.

3.4. Dynamic Vapor Sorption

We previously showed that cocrystallization of CUR with PHL effectively alleviated the phase transformation of PHL anhydrate into its dihydrate [24]. Such reduction in hygroscopicity is crucial in ensuring the adequate stability of the solid forms, which facilitates the successful pharmaceutical development. Crystal hydration may also alter solubility, dissolution performance, manufacturability, and shelf-life of drug substance. Therefore, the hygroscopicity of CUR, coformers, and their corresponding cocrystals was compared.

The moisture sorption of CUR was minimal due to its non-hygroscopic nature [24], whilst some of the coformers sorbed a considerable amount of water in the 85-95% RH range (Figure 6). At 95% RH, RES, HXQ, PYR, and CUR-HXQ showed signs of deliquesce while CUR-RES and CUR-PYR did not. Thus, cocrystallization improved stability of RES and PYR against high RH (Figure S3). The improvement in hygroscopicity observed in the cocrystals may be explained by the fact that the phenolic groups present in benezenediols and benezenetriols predominantly participated in pheno−phenol and/or phenol−carbonyl intermolecular hydrogen bonding interaction with curcumin upon cocrystallization. This rendered the interaction, via O−H···O hydrogen bonds between the phenolic groups and water vapor molecules, less favorable. The stronger crystal lattice, indicated by the higher molar enthalpy of fusion of the cocrystals, possibly contributed to their better stability against moisture. Another factor that affects hygroscopicity is molecular hydrophilicity. Both the much higher hydrophobicity and relatively high molar enthalpy of fusion contribute to its very low hygroscopicity.

It is interesting to note that, CAT (Figure S3a) showed unusual weight change during the DVS experiments, where weight continued to decrease throughout the experiment even when RH was increased. This indicates sublimation of CAT, where the loss of solid CAT to the purging gas, due to its high vapor pressure, exceeded weight gained due to increased RH. In order to obtain more accurate moisture sorption data, an average sublimation rate of CAT was calculated based on weight loss data under a similar flow rate of dry nitrogen purge (Figure S4). The corrected moisture sorption isotherm of CAT is considerably improved (Figure 6b and S3a).

The DVS results indicated that, at 80% RH, none of the cocrystals adsorbed a significant amount of water (Table 3). The slight differences may be attributed to different surface areas among the samples. At 95% RH, the amount of adsorbed water followed the descending order of CUR-CAT > CUR-PYR > CUR-HYQ (> CUR) > CUR-RES > CUR-HXQ. This order is not exactly the same as that of coformers, which is CAT > HYQ (> CUR) > PYR > HXQ > RES. The hygroscopicity of coformers and cocrystals cannot be simply correlated to the number of hydroxyl groups in the coformer structures, which is CAT = RES = HYQ < PYR = HXQ. This is not surprising since

hygroscopicity of the crystals is related not only to their molecular structures but also intermolecular interactions in crystal, where strongly interacting molecules in the crystals are less easily accessible by water.

3.5. Intrinsic Dissolution Rate (IDR) Measurement

One of the advantages of cocrystallization of poorly water-soluble drugs, especially with highly water soluble coformers, is their potentially favorable dissolution rate and bioavailability. However, such soluble cocrystals often risk precipitation of the poorly soluble parent drugs during dissolution, which makes it difficult to measure the solubility of cocrystals. Intrinsic dissolution rate (IDR) measurement is a useful alternative approach to estimate solubility improvement by cocrystals, from which propensity to phase change during dissolution can also be assessed based on how quickly dissolution curve deviates from linearity.

For CUR-CAT, CUR-RES, CUR-HYQ, CUR-PYR, and CUR-PHL systems, after the initial fast release of CUR into the medium, the slope quickly decreased to a constant corresponding to that of CUR (Figure 7a, b, c, e, and [24]). The IDR curves strongly suggested rapid phase transformation of the cocrystals to CUR, sometimes in a matter of few seconds, upon contact with the dissolution medium. Due to very fast phase transformation occurred, few data points could be recorded to provide a reliable IDR value. In those cases, the slope of the terminal linear portion was reported in Table 4. All terminal IDR values were comparable to that of CUR, suggesting the coating of pellet surface by CUR after the initial stage of the dissolution process. This was confirmed by X-ray diffractograms of the CUR-CAT pellet after IDR study (Figure S5a), which showed characteristic peak of CUR, e.g., 12.33°, 17.25°, while the intensity of characteristic peaks corresponding to CUR-CAT cocrystal (10.58°, 10.95°, 11.87° and 18.77°) significantly decreased. This confirms that CUR has precipitated out and deposited onto the surface of the dissolving pellet of the cocrystal. Similar to CUR-PHL cocrystal [24], the phase change was also visually observed based on the color change of the pellets (Figure 8), where the side in contact with dissolution medium turned lighter yellow color after IDR experiment while the punch side remained darker red color of the corresponding cocrystals.

The driving force of the precipitation of CUR is its high concentration in the diffusion layer due to the dissolution of the more soluble cocrystals. However, the high degree of supersaturation led to formation of the poorly water-soluble CUR quickly [56], which coated surface of the cocrystal pellet. Such fast precipitation negates solubility improvement by cocrystallization, which must be inhibited in order to reap the potential solubility advantage of cocrystals. Formulation strategies include using suitable polymers and excess common coformers [57]. While in the case of CUR-HXQ (Figure 7d), the IDR value was significantly higher (7x) than other systems (Table 4), no evidence of phase transformation was suggested by XRD pattern (Figure S5b). The improvement in dissolution rate was attributed to the higher stability of CUR-HXQ, where the rate of phase change from cocrystal to the API was much lower.

The IDR results indicated that, when using cocrystallization approach to improve dissolution for a poorly soluble drug, it is important to consider not only the solubility of the coformer but also the phase stability during dissolution.

3.6. Tabletability

Tabletability of drugs plays an important role in manufacturing tablet products. Accordingly, tabletability of these cocrystals was evaluated for the feasibility of tablet product development because CUR is poorly compressible and does not form intact tablets at the compaction pressures ranging from 50 MPa to 350 MPa [24]. All five CUR cocrystals showed much better tabletability compared to CUR (Figure 9). The tensile strength of all five cocrystals reached 2 MPa below 300 MPa compaction pressure. In fact, the tensile strength of 2 MPa was readily achievable at around 150 MPa for CUR-RES, CUR-HYQ, CUR-HXQ, and CUR-PYR. Thus, these cocrystals are not expected to have tableting problems even at a high drug loading [58]. While the tabletability of the CUR-PYR cocrystal is comparable with that of PYR, all other four cocrystals exhibited higher tabletability than corresponding coformers as well (Figure S6). The synergistic effects again confirmed the effectiveness of improving tabletability by cocrystallization [24, 59-62]. Such effects likely have their origins in unique crystal structures of the cocrystals in relation to the coformers [63].

3.7. Significance of the Study

This work demonstrates the effectiveness of rapid solvent removal approach in preparing otherwise elusive cocrystals. These CUR cocrystals largely retained the low hygroscopicity of CUR while reducing hygroscopicity of individual coformers. CUR-HXQ exhibited 7 times faster intrinsic dissolution rate than CUR. Other cocrystals underwent fast precipitation of CUR during the dissolution process, which negated the solubility improvement by cocrystallization. All five cocrystals had better tabletability than CUR. This work exemplifies the usefulness of cocrystallization in solving pharmaceutical deficiencies of problematic drugs to facilitate successful tablet product development.

4. Conclusion

Using rotary evaporation of acetone solutions, phase pure 1:1 cocrystals of curcumin with five structurally similar benezenediols and benezenetriols were successfully prepared, including the elusive CUR-HYQ and CUR-CAT cocrystals. Compared to individual coformers, some cocrystals displayed lower hygroscopicity, faster dissolution rate, or better tableting performance. Overall, CUR-HXQ appears to be a good candidate for future development of tablet products of CUR.

Acknowledgements

The work was financially supported by the Li Ka Shing Faculty of Medicine (Project number 204600519) and University Research Committee (Project number 104004777) at The University of Hong Kong.

Supporting Information

Equilibrium solubilities of CUR and the polyphenolic coformers in acetone, PXRD patterns of CUR cocrystals produced by slow evaporation in acetone, Physical stability of CUR cocrystals revealed by PXRD patterns, DVS isotherms of CUR cocrystal systems and the polyphenolic coformers, Sublimation of CAT, Phase transformation of

CUR cocrystals during IDR studies revealed by PXRD patterns, Tabletability of CUR, the chosen polyphenolic coformers and each CUR cocrystal systems.

References

1. Aitipamula, S.; Banerjee, R.; Bansal, A. K.; Biradha, K.; Cheney, M. L.; Choudhury, A. R.; Desiraju, G. R.; Dikundwar, A. G.; Dubey, R.; Duggirala, N., Polymorphs, salts, and cocrystals: What's in a name? *Cryst. Growth Des.* **2012,** *12*, 2147-2152.
2. U.S. Food and Drug Administration, C. f. D. E. a. R. C., Regulatory Classification of Pharmaceutical Co-Crystals Guidance for Industry. Revision 1 ed.; Washington, DC, 2016.
3. Schultheiss, N.; Newman, A., Pharmaceutical cocrystals and their physicochemical properties. *Cryst. Growth Des.* **2009,** *9*, 2950-2967.
4. Jones, W.; Motherwell, W. S.; Trask, A. V., Pharmaceutical cocrystals: an emerging approach to physical property enhancement. *MRS Bull.* **2006,** *31*, 875-879.
5. Blagden, N.; De Matas, M.; Gavan, P.; York, P., Crystal engineering of active pharmaceutical ingredients to improve solubility and dissolution rates. *Adv. Drug Delivery Rev.* **2007,** *59*, 617-630.
6. Karki, S.; Friščić, T.; Fábián, L.; Laity, P. R.; Day, G. M.; Jones, W., Improving mechanical properties of crystalline solids by cocrystal formation: new compressible forms of paracetamol. *Adv. Mater.* **2009,** *21*, 3905-3909.
7. Chow, S. F.; Chen, M.; Shi, L.; Chow, A. H.; Sun, C. C., Simultaneously improving the mechanical properties, dissolution performance, and hygroscopicity of ibuprofen and flurbiprofen by cocrystallization with nicotinamide. *Pharm. Res.* **2012,** *29*, 1854-65.
8. Sun, C. C., Cocrystallization for successful drug delivery. *Expert Opin. Drug Delivery* **2013,** *10*, 201-13.
9. Duggirala, N. K.; Perry, M. L.; Almarsson, O.; Zaworotko, M. J., Pharmaceutical cocrystals: along the path to improved medicines. *Chem Commun (Camb)* **2016,** *52*, 640-55.
10. Trask, A. V., An overview of pharmaceutical cocrystals as intellectual property. *Mol. Pharmaceutics* **2007,** *4*, 301-309.
11. Thipparaboina, R.; Kumar, D.; Chavan, R. B.; Shastri, N. R., Multidrug co-crystals: towards the development of effective therapeutic hybrids. *Drug Discovery Today* **2016,** *21*, 481-490.
12. Brantley, S.; Argikar, A.; Lin, Y. S.; Nagar, S.; Paine, M. F., Herb-drug interactions: challenges and opportunities for improved predictions. *Drug Metab. Dispos.* **2014**, *42*, 301-317.
13. Chen, J. M.; Li, S.; Lu, T. B., Pharmaceutical Cocrystals of Ribavirin with Reduced Release Rates. *Cryst. Growth Des.* **2014,** *14*, 6399-6408.
14. Chen, Y. M.; Rodríguez-Hornedo, N., Cocrystals Mitigate Negative Effects of High pH on Solubility and Dissolution of a Basic Drug. *Cryst. Growth Des.* **2018,** *18*, 1358-1366.

15. Trask, A. V.; Jones, W., Crystal engineering of organic cocrystals by the solid-state grinding approach. *Org. Solid-State React.* **2005**, 131-131.
16. Basavoju, S.; Boström, D.; Velaga, S. P., Indomethacin–saccharin cocrystal: design, synthesis and preliminary pharmaceutical characterization. *Pharm. Res.* **2008,** *25*, 530-541.
17. Mutalik, S.; Anju, P.; Manoj, K.; Usha, A. N., Enhancement of dissolution rate and bioavailability of aceclofenac: a chitosan-based solvent change approach. *Int. J. Pharm.* **2008,** *350*, 279-290.
18. Takata, N.; Shiraki, K.; Takano, R.; Hayashi, Y.; Terada, K., Cocrystal screening of stanolone and mestanolone using slurry crystallization. *Cryst. Growth Des.* **2008,** *8*, 3032-3037.
19. Berry, D. J.; Seaton, C. C.; Clegg, W.; Harrington, R. W.; Coles, S. J.; Horton, P. N.; Hursthouse, M. B.; Storey, R.; Jones, W.; Friscic, T., Applying hot-stage microscopy to co-crystal screening: a study of nicotinamide with seven active pharmaceutical ingredients. *Cryst. Growth Des.* **2008,** *8*, 1697-1712.
20. Thakur, T. S.; Desiraju, G. R., Crystal Structure Prediction of a Co-Crystal Using a Supramolecular Synthon Approach: 2-Methylbenzoic Acid− 2-Amino-4-methylpyrimidine. *Cryst. Growth Des.* **2008,** *8*, 4031-4044.
21. Mohammad, M. A.; Alhalaweh, A.; Velaga, S. P., Hansen solubility parameter as a tool to predict cocrystal formation. *Int. J. Pharm.* **2011,** *407*, 63-71.
22. Abramov, Y. A.; Loschen, C.; Klamt, A., Rational coformer or solvent selection for pharmaceutical cocrystallization or desolvation. *J. Pharm. Sci.* **2012,** *101*, 3687-3697.
23. Springuel, G. r.; Norberg, B.; Robeyns, K.; Wouters, J.; Leyssens, T., Advances in pharmaceutical co-crystal screening: effective co-crystal screening through structural resemblance. *Cryst. Growth Des.* **2011,** *12*, 475-484.
24. Chow, S. F.; Shi, L.; Ng, W. W.; Leung, K. H. Y.; Nagapudi, K.; Sun, C. C.; Chow, A. H., Kinetic entrapment of a hidden curcumin cocrystal with phloroglucinol. *Cryst. Growth Des.* **2014,** *14*, 5079-5089.
25. Alhalaweh, A.; Velaga, S. P., Formation of cocrystals from stoichiometric solutions of incongruently saturating systems by spray drying. *Cryst. Growth Des.* **2010,** *10*, 3302-3305.
26. Motterlini, R.; Foresti, R.; Bassi, R.; Green, C. J., Curcumin, an antioxidant and anti-inflammatory agent, induces heme oxygenase-1 and protects endothelial cells against oxidative stress. *Free Radical Biol. Med.* **2000,** *28*, 1303-1312.
27. Aggarwal, B. B.; Harikumar, K. B., Potential therapeutic effects of curcumin, the anti-inflammatory agent, against neurodegenerative, cardiovascular, pulmonary, metabolic, autoimmune and neoplastic diseases. *Int. J. Biochem. Cell Biol.* **2009,** *41*, 40-59.
28. Rai, D.; Singh, J. K.; Roy, N.; Panda, D., Curcumin inhibits FtsZ assembly: an attractive mechanism for its antibacterial activity. *Biochem. J* **2008,** *410*, 147-155.
29. Martins, C.; Da Silva, D.; Neres, A.; Magalhaes, T.; Watanabe, G.; Modolo, L.; Sabino, A.; De Fátima, A.; De Resende, M., Curcumin as a promising antifungal of clinical interest. *J. Antimicrob. Chemother.* **2008,** *63*, 337-339.
30. Itthipanichpong, C.; Ruangrungsi, N.; Kemsri, W.; Sawasdipanich, A., Antispasmodic effects of curcuminoids on isolated guinea-pig ileum and rat uterus. *J. Med. Assoc. Thailand* **2003,** *86*, S299-309.

31. Babu, P. S.; Srinivasan, K., Hypolipidemic action of curcumin, the active principle of turmeric (Curcuma longa) in streptozotocin induced diabetic rats. *Mol. Cell. Biochem.* **1997,** *166*, 169-175.
32. Ishrat, T.; Hoda, M. N.; Khan, M. B.; Yousuf, S.; Ahmad, M.; Khan, M. M.; Ahmad, A.; Islam, F., Amelioration of cognitive deficits and neurodegeneration by curcumin in rat model of sporadic dementia of Alzheimer's type (SDAT). *Eur. Neuropsychopharmacol.* **2009,** *19*, 636-647.
33. Thiyagarajan, M.; Sharma, S. S., Neuroprotective effect of curcumin in middle cerebral artery occlusion induced focal cerebral ischemia in rats. *Life Sci.* **2004,** *74*, 969-985.
34. García-Niño, W. R.; Pedraza-Chaverrí, J., Protective effect of curcumin against heavy metals-induced liver damage. *Food Chem. Toxicol.* **2014,** *69*, 182-201.
35. Aguilar, F.; Dusemund, B.; Galtier, P.; Gilbert, J.; Gott, D.; Grilli, S.; Gürtler, R.; König, J.; Lambré, C.; Larsen, J., Scientific opinion on the re-evaluation of curcumin (E 100) as a food additive. *EFSA J* **2010,** *8*, 46.
36. Lao, C. D.; Ruffin, M. T.; Normolle, D.; Heath, D. D.; Murray, S. I.; Bailey, J. M.; Boggs, M. E.; Crowell, J.; Rock, C. L.; Brenner, D. E., Dose escalation of a curcuminoid formulation. *BMC Complementary Altern. Med.* **2006,** *6*, 10.
37. Additives, J. F. W. E. C. o. F.; Organization, W. H., *Evaluation of certain food additives and contaminants: sixty-first report of the joint FAO/WHO expert committee on food additives*. World Health Organization: 2004; Vol. 61.
38. Kunnumakkara, A. B.; Bordoloi, D.; Padmavathi, G.; Monisha, J.; Roy, N. K.; Prasad, S.; Aggarwal, B. B., Curcumin, the golden nutraceutical: multitargeting for multiple chronic diseases. *Br. J. Pharmacol.* **2017,** *174*, 1325-1348.
39. Tønnesen, H. H.; Másson, M.; Loftsson, T., Studies of curcumin and curcuminoids. XXVII. Cyclodextrin complexation: solubility, chemical and photochemical stability. *Int. J. Pharm.* **2002,** *244*, 127-135.
40. Nelson, K. M.; Dahlin, J. L.; Bisson, J.; Graham, J.; Pauli, G. F.; Walters, M. A., The essential medicinal chemistry of curcumin: miniperspective. *J. Med. Chem.* **2017,** *60*, 1620-1637.
41. Sanphui, P.; Goud, N. R.; Khandavilli, U. R.; Nangia, A., Fast dissolving curcumin cocrystals. *Cryst. Growth Des.* **2011,** *11*, 4135-4145.
42. Perron, N. R.; Brumaghim, J. L., A review of the antioxidant mechanisms of polyphenol compounds related to iron binding. *Cell Biochem. Biophys.* **2009,** *53*, 75-100.
43. Cowan, M. M., Plant products as antimicrobial agents. *Clin. Microbiol. Rev.* **1999,** *12*, 564-582.
44. Sun, C.; Grant, D. J., Effects of initial particle size on the tableting properties of L-lysine monohydrochloride dihydrate powder. *Int J Pharm* **2001,** *215*, 221-8.
45. Sun, C.; Grant, D. J., Influence of crystal shape on the tableting performance of L-lysine monohydrochloride dihydrate. *J Pharm Sci* **2001,** *90*, 569-79.
46. Paul, S.; Chang, S.-Y.; Sun, C. C., The phenomenon of tablet flashing — Its impact on tableting data analysis and a method to eliminate it. *Powder Technol.* **2017,** *305*, 117-124.
47. Fell, J. T.; Newton, J. M., Determination of tablet strength by the diametral-compression test. *J Pharm Sci* **1970,** *59*, 688-91.

48. Sathisaran, I.; Dalvi, S. V., Crystal engineering of curcumin with salicylic acid and hydroxyquinol as coformers. *Cryst. Growth Des.* **2017,** *17*, 3974-3988.
49. Goud, N. R.; Suresh, K.; Sanphui, P.; Nangia, A., Fast dissolving eutectic compositions of curcumin. *Int. J. Pharm.* **2012,** *439*, 63-72.
50. Lee, E. H., A practical guide to pharmaceutical polymorph screening & selection. *Asian J. Pharm. Sci.* **2014,** *9*, 163-175.
51. Ostwald, W., Studies on formation and transformation of solid materials. *Z. Phys. Chem.* **1897,** *22*, 289–330.
52. Burger, A.; Ramberger, R., On the polymorphism of pharmaceuticals and other molecular crystals. I. *Microchim. Acta* **1979,** *72*, 259-271.
53. Yamashita, H.; Hirakura, Y.; Yuda, M.; Terada, K., Coformer screening using thermal analysis based on binary phase diagrams. *Pharm. Res.* **2014,** *31*, 1946-1957.
54. Cherukuvada, S.; Guru Row, T. N., Comprehending the formation of eutectics and cocrystals in terms of design and their structural interrelationships. *Cryst. Growth Des.* **2014,** *14*, 4187-4198.
55. Yamashita, H.; Hirakura, Y.; Yuda, M.; Teramura, T.; Terada, K., Detection of cocrystal formation based on binary phase diagrams using thermal analysis. *Pharm. Res.* **2013,** *30*, 70-80.
56. Yamashita, H.; Sun, C. C., Harvesting Potential Dissolution Advantages of Soluble Cocrystals by Depressing Precipitation Using the Common Coformer Effect. *Cryst. Growth Des.* **2016,** *16*, 6719-6721.
57. Yamashita, H.; Sun, C. Q. C., Self-templating accelerates precipitation of carbamazepine dihydrate during the dissolution of a soluble carbamazepine cocrystal. *Crystengcomm* **2017,** *19*, 1156-1159.
58. C.C. Sun, H. H., P. Gao, C. Ma, C. Medina, F. Alvarez. , Development and optimization of high drug load tablet formulation based on assessment of powder manufacturability – moving towards quality by design. *J Pharm Sci* **2009,** *98*, 239-247.
59. Sun, C. C.; Hou, H., Improving mechanical properties of caffeine and methyl gallate crystals by cocrystallization. *Cryst. Growth Des.* **2008,** *8*, 1575-1579.
60. Perumalla, S. R.; Paul, S.; Sun, C. C., Enabling the Tablet Product Development of 5-Fluorocytosine by Conjugate Acid Base Cocrystals. *J Pharm Sci* **2016,** *105*, 1960-1966.
61. Wang, Z. Z.; Chen, J. M.; Lu, T. B., Enhancing the Hygroscopic Stability of S-Oxiracetam via Pharmaceutical Cocrystals. *Cryst. Growth Des.* **2012,** *12*, 4562-4566.
62. Deng, J. H.; Lu, T. B.; Sun, C. C.; Chen, J. M., Dapagliflozin-citric acid cocrystal showing better solid state properties than dapagliflozin. *Eur J Pharm Sci* **2017,** *104*, 255-261.
63. L. Liu, C. W., J. Dun, A.H L. Chow, and C.C. Sun, Lack of dependence of mechanical properties of baicalein cocrystals on those of the constituent components. *CrystEngComm*. **2018,** http://dx.doi.org/10.1039/C8CE00787J

Table 1. Melting temperature and heat of fusion of CUR, the chosen polyphenolic coformers, and each CUR cocrystal systems (n = 3).

Sample	Melting point (^{o}C)	Eutectics melting (^{o}C)	ΔH_f (kJ/mol)
Curcumin*	183.2 ± 0.2	—	50.0 ± 0.4
CAT	104.9 ± 0.3	—	28.5 ± 0.2
RES	109.7 ± 0.6	—	22.1 ± 0.2
HYQ	173.0 ± 0.3	—	26.9 ± 0.2
HXQ	141.6 ± 0.3	—	36.2 ± 0.4
PHL	218.3 ± 0.4	—	33.5 ± 0.3
PYR	131.1 ± 0.2	—	26.3 ± 0.2
CUR-CAT	152.0 ± 0.3	142.4, 91.9	72.0 ± 0.5
CUR-RES	171.2 ± 1.0	162.8, 90.3	63.8 ± 1.0
CUR-HYQ	157.9 ± 1.8	152.1, 147.3	51.7 ± 0.8
CUR-HXQ	165.0 ± 0.5	155.1, 126.5	73.9 ± 1.2
CUR-PHL*	179.9 ± 0.7	173.6, 170.1	58.9 ± 1.1
CUR-PYR	165.7 ± 1.6	158.4, 124.3	60.3 ± 0.9

* Ref. [24]

Table 2. Key features in the FTIR spectra of CUR, the chosen polyphenolic coformers, and each CUR cocrystal systems.

Sample	Phenolic O-H stretching / cm^{-1}	C=O stretching / cm^{-1}	Aromatic C=C / cm^{-1}
CUR*	3506	1628	1603
CAT	3451, 3329	—	1599
RES	3261	—	1609
HYQ	3263	—	1609
HXQ	3278	—	1573
PHL	3203	—	1618
PYR	3433	—	1619
CUR-CAT	3449, 3409	1626	1591
CUR-RES	3437	1625	1604
CUR-HYQ	3432	1629	1605
CUR-HXQ	3423	1628	1587
CUR-PHL*	3412	1625	1609, 1592
CUR-PYR	3401	1624	1591

* Ref. [24]

Table 3. The amount of sorbed water (%) in the samples at 80% RH and 95% RH.

	80% RH			**95% RH**		
	cocrystal	coformer	% difference	cocrystal	coformer	%difference
CUR	NA	0.36	NA	NA	0.98	NA
CAT	0.14	0.01	+0.13	0.21	0.16	+0.05
RES	0.57	0.04	+0.53	1.60	92.66	-91.06
HYQ	0.33	0.16	+0.17	0.80	0.46	+0.34
HXQ	0.78	0.24	+0.54	18.79	26.67	-7.88
PYR	0.37	0.07	+0.30	0.76	15.92	-15.16

Table 4. IDR data of Curcumin and its five cocrystals.

Intrinsic dissolution rate ($ug \cdot cm^{-2} \cdot min^{-1}$)					
	Tablet 1	Tablet 2	Tablet 3	Average	SD
CUR	50.1	55.6	62.1	**55.9**	6.0
CUR-CAT	52.2	52.9	50.8	**52.0**	1.1
CUR-RES	45.2	45.3	42.0	**44.2**	1.9
CUR-HYQ	49.8	49.1	50.5	**49.8**	0.7
CUR-HXQ	339.0	373.0	314.3	**342.1**	29.5
CUR-PYR	45.7	47.7	46.4	**46.6**	1.0

Enol Curcumin

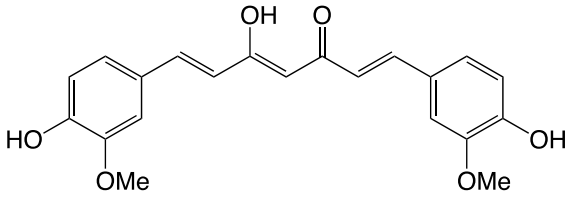

Benzenediol **Benzenetriol**

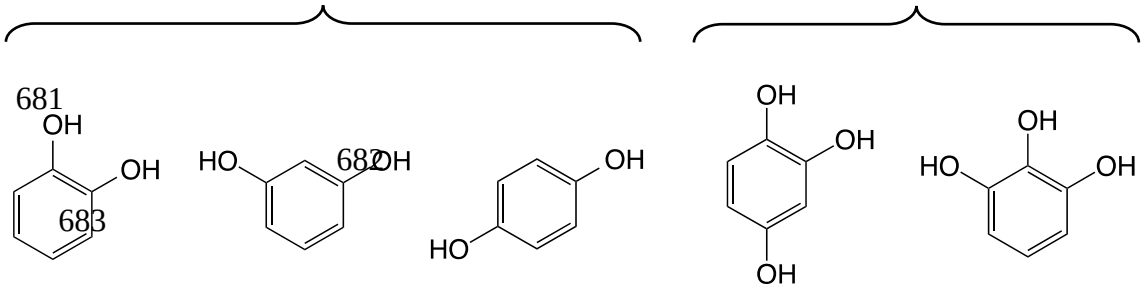

Catechol (CAT) ***Resorcinol (RES)*** ***Hydroquinone (HYQ)*** ***Hydroxyquinol (HXQ)*** ***Pyrogallol (PYR)***

Figure 1. Chemical structures of enol curcumin and the chosen polyphenolic coformers.

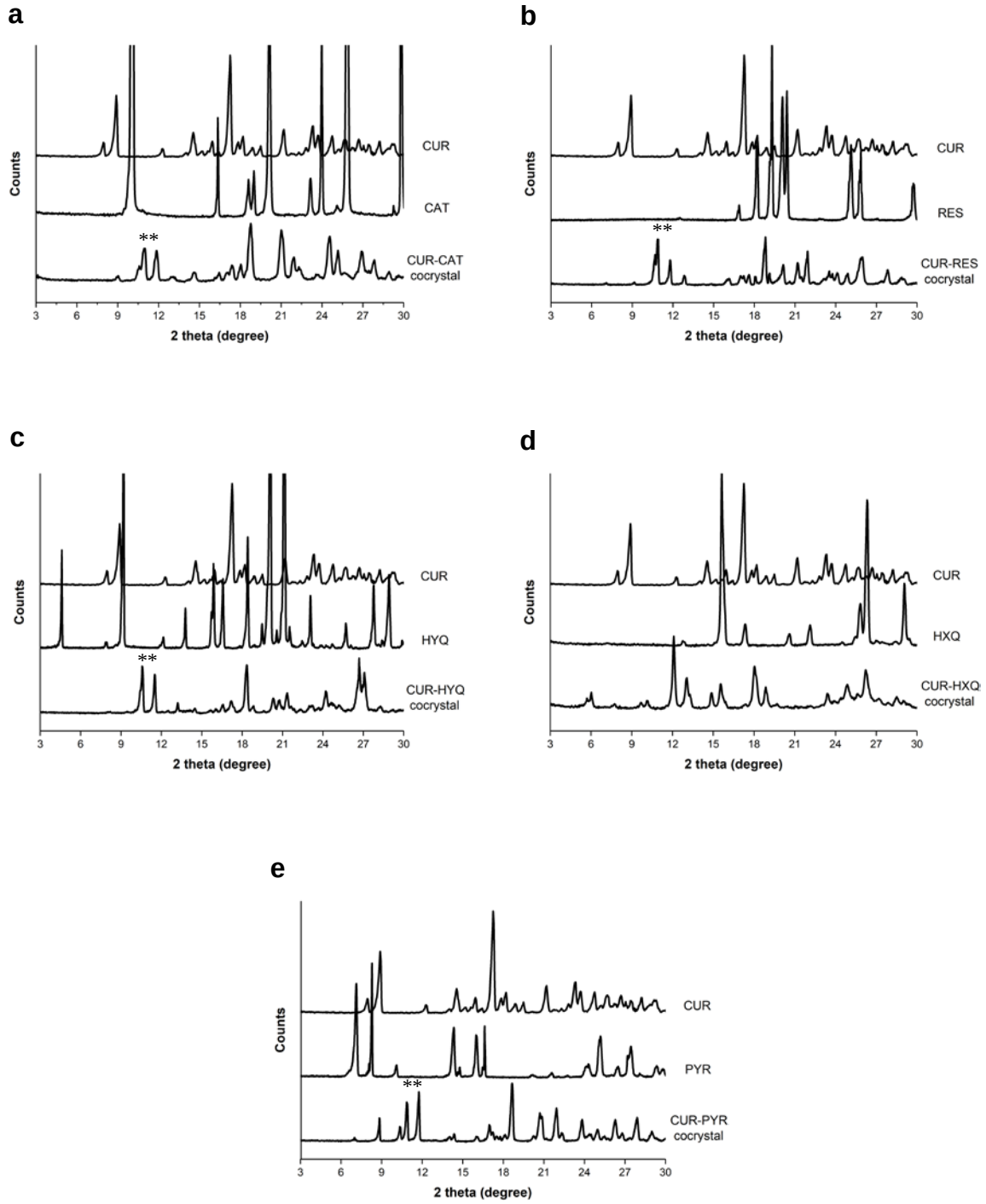

Figure 2. PXRD patterns of (a) CUR-CAT, (b) CUR-RES, (c) CUR-HYQ, (d) CUR-HXQ and (e) CUR-PYR cocrystal systems in a 1:1 stoichiometric ratio. Peaks at similar 2 theta angles are marked with *.

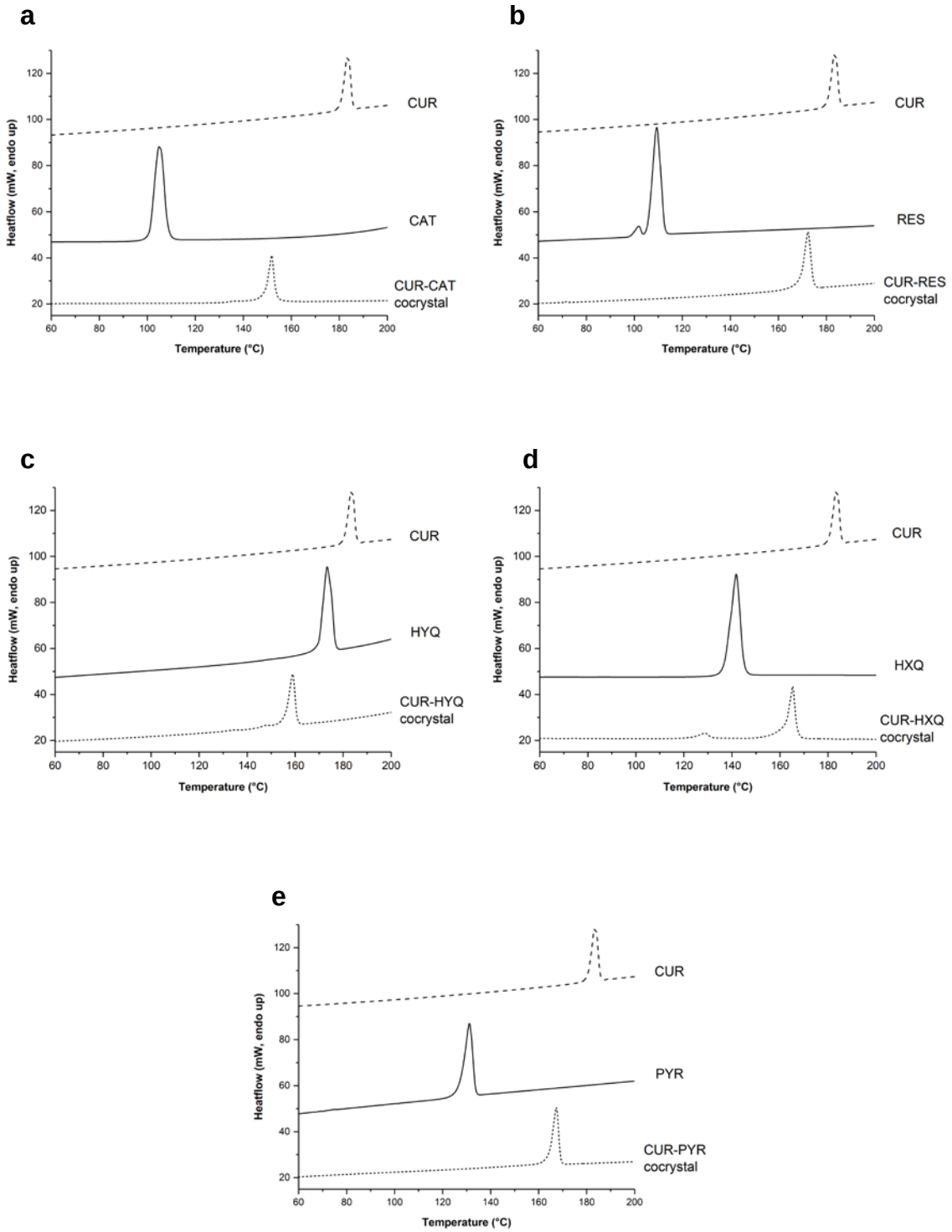

Figure 3. DSC profiles of CUR 1:1 cocrystal systems, (a) CUR-CAT, (b) CUR-RES, (c) CUR-HYQ, (d) CUR-HXQ and (e) CUR-PYR.

a

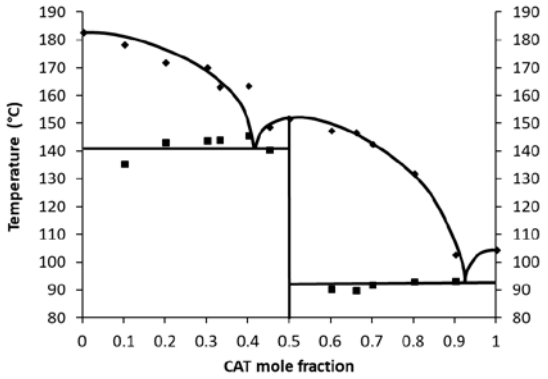
Temperature (°C)
CAT mole fraction

b

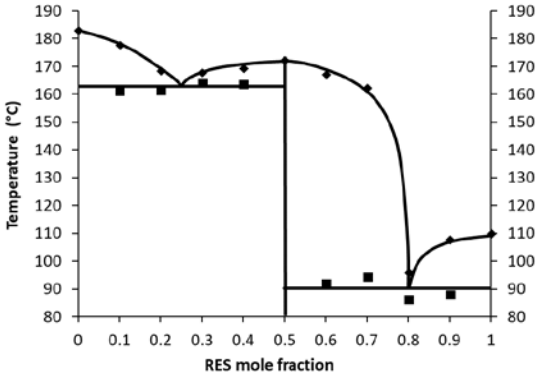
Temperature (°C)
RES mole fraction

c

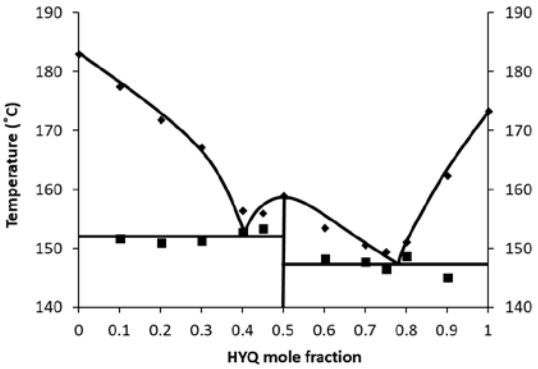
Temperature (°C)
HYQ mole fraction

d

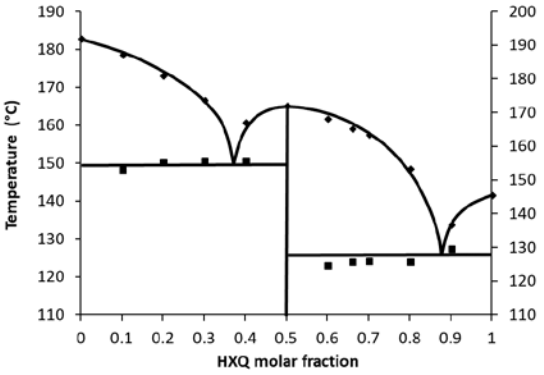
Temperature (°C)
HXQ molar fraction

e

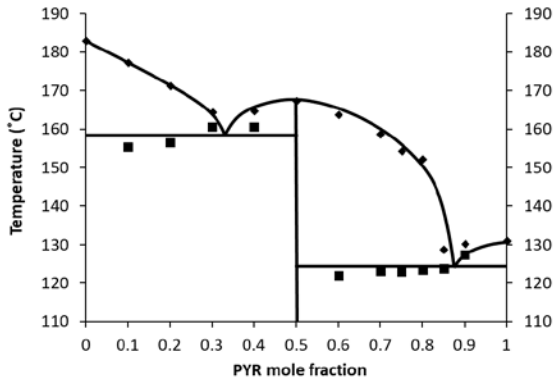

Figure 4. Melting point – composition phase diagrams of CUR 1:1 cocrystal systems, (a) CUR-CAT, (b) CUR-RES, (c) CUR-HYQ, (d) CUR-HXQ, and (e) CUR-PYR.

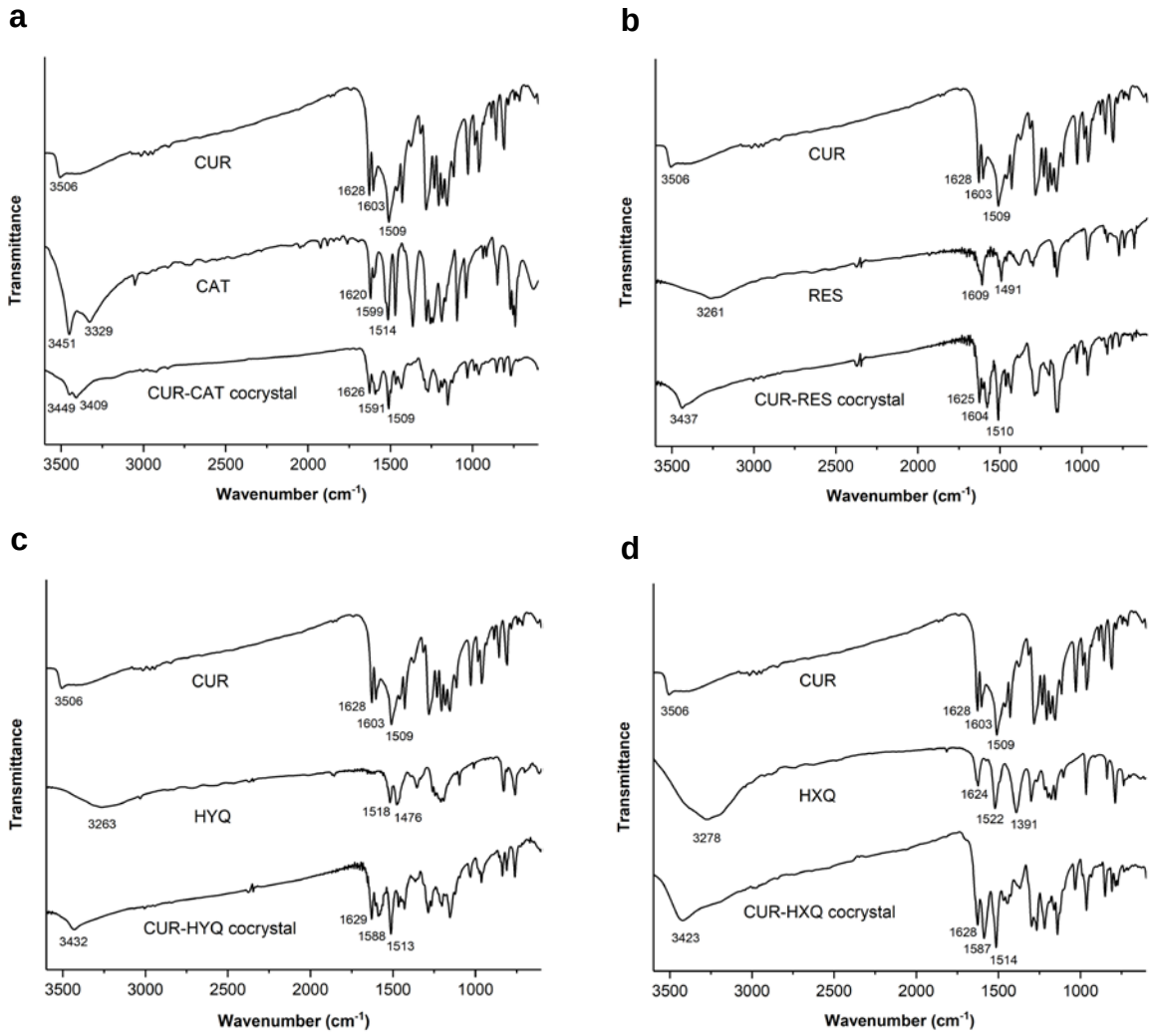

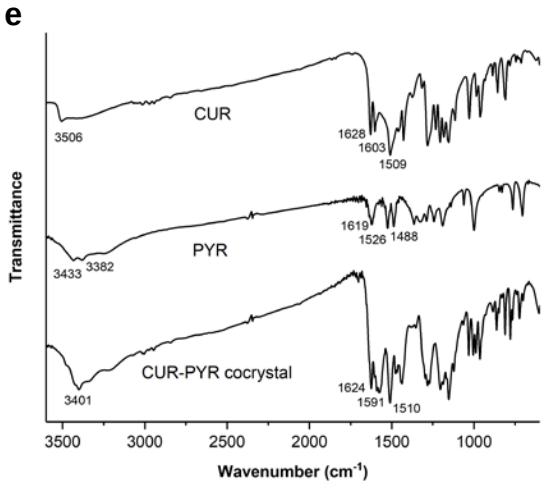

Figure 5. FTIR spectra of CUR 1:1 cocrystal systems, (a) CUR-CAT, (b) CUR-RES, (c) CUR-HYQ, (d) CUR-HXQ, and (e) CUR-PYR.

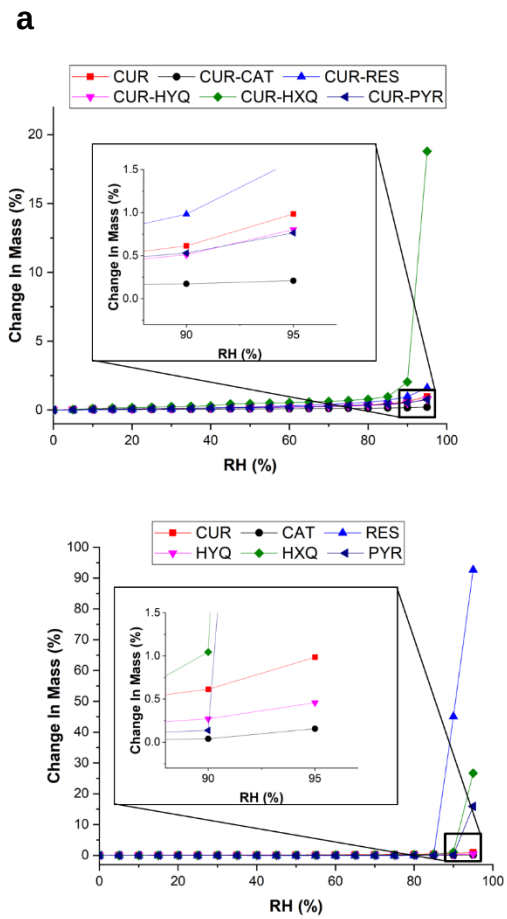

Figure 6. Water sorption isotherms at 25 ^{o}C of CUR and different powders, (a) five cocrystals and (b) five polyphenolic coformers.

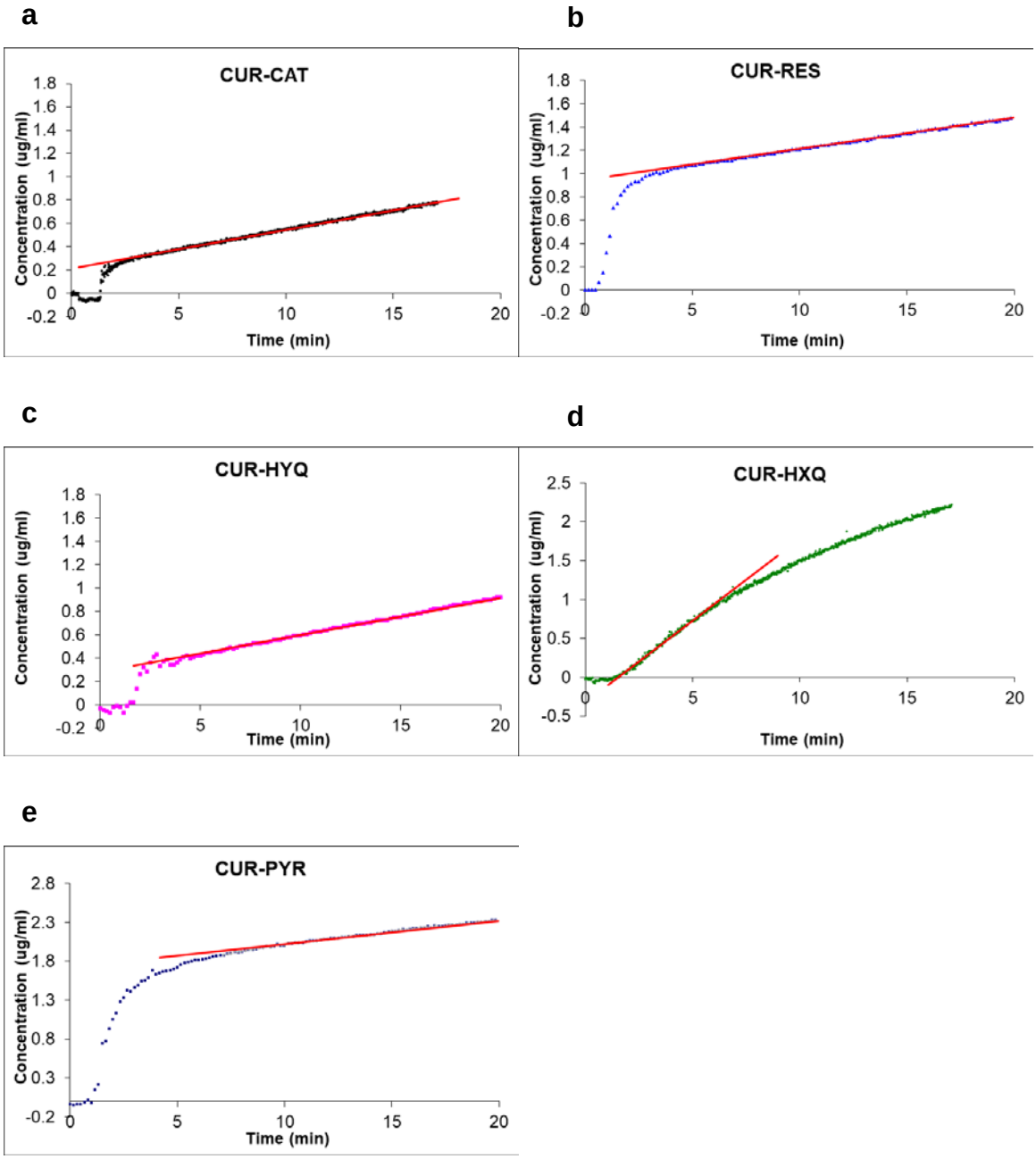

Figure 7. IDR curves of five CUR cocrystals a) CUR-CAT, b) CUR-RES, c) CUR-HYQ, d) CUR-HXQ, and e) CUR-PYR. The regression lines used for determining IDR are shown.

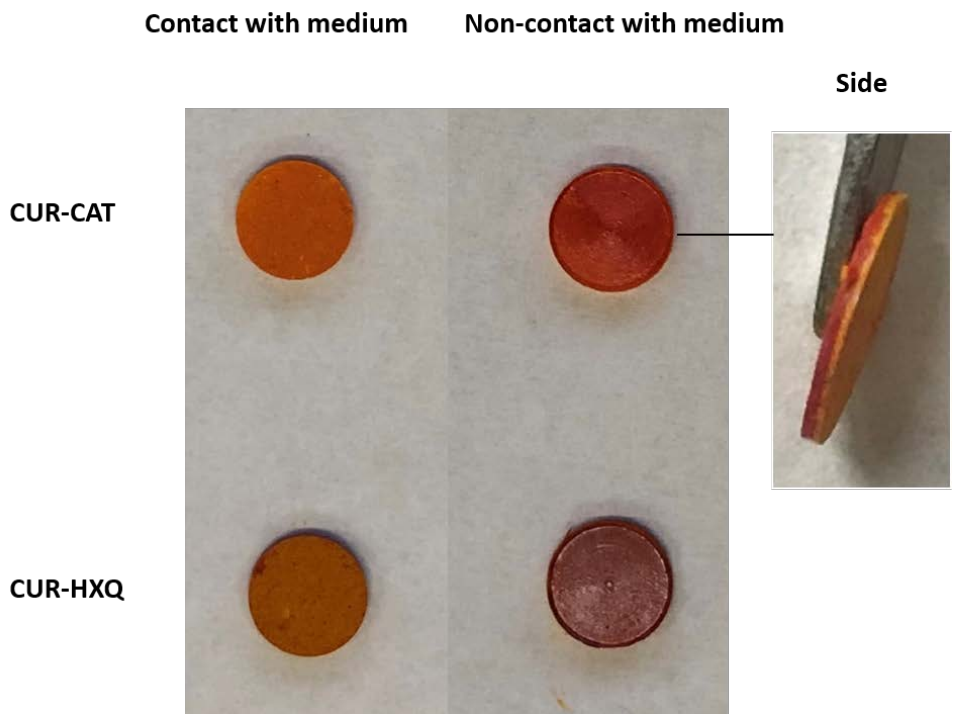

Figure 8. Color change of cocrystals upon contacting with dissolution medium.

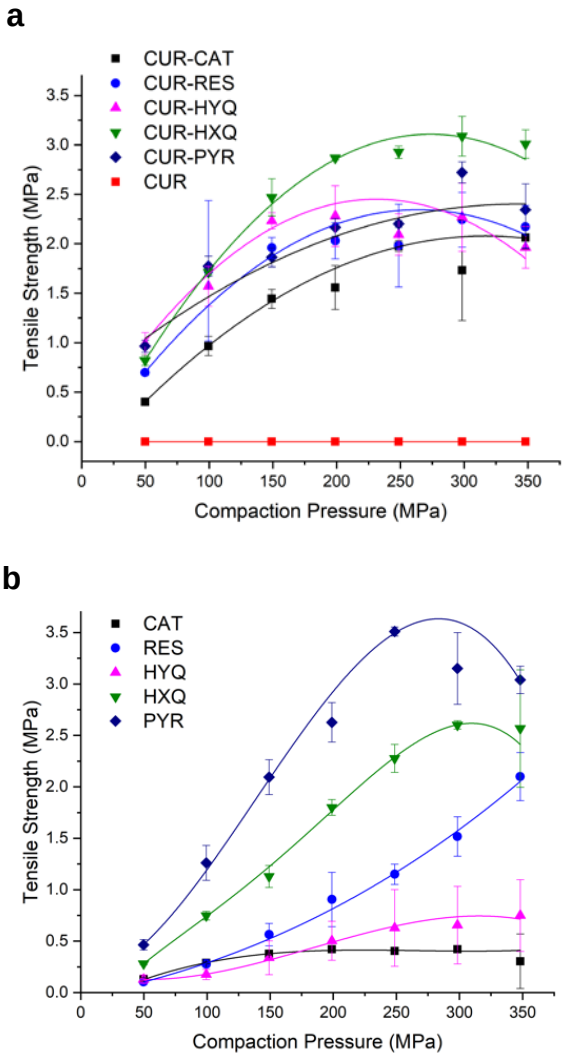

Figure 9. Tabletability profiles of different powders, a) CUR and the five cocrystals; b) polyphenolic coformers.

For Table of Contents Use Only,

Cocrystallization of curcumin with benzenediols and benzenetriols via rapid solvent removal

Si Nga Wong[1,#], Shenye Hu[2,#], Wai Wing Ng[3], Xiaoyan Xu[1], Ka Lun Lai[3], Wai Yip Thomas Lee[4], Albert Hee Lum Chow[3], Changquan Calvin Sun[2,*], Shing Fung Chow[1,*]

Synopsis:

Rapid solvent removal is an effective approach for screening elusive cocrystals, particularly through selecting structurally resemble coformers. We herein report the successful preparation of two new phase pure 1:1 cocrystals of curcumin with catechol, and hydroquinone, and a new polymorph of cocrystal with hydroxyquinol with improved pharmaceutical properties.

TOC graphic:

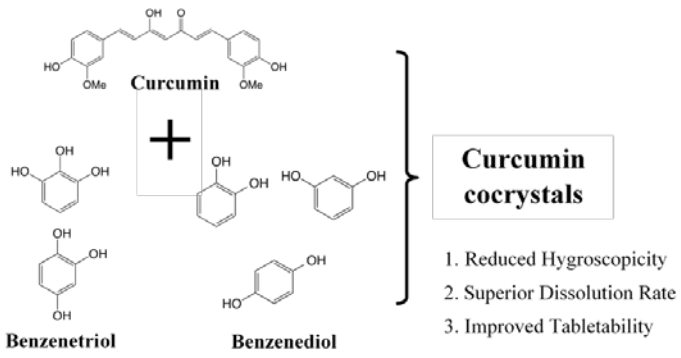

Supporting Information

Cocrystallization of curcumin with benzenediols and benzenetriols via rapid solvent removal

Si Nga Wong[1,#], Shenye Hu[2,#], Wai Wing Ng[3], Xiaoyan Xu[1], Ka Lun Lai[3], Wai Yip Thomas Lee[4], Albert Hee Lum Chow[3], Changquan Calvin Sun[2,*], Shing Fung Chow[1,*]

Table S1. Equilibrium solubilities of CUR and the polyphenolic coformers in acetone at 25 °C (n=3).

	Solubility in Acetone (mM)
Curcumin*	136.7 ± 6.92
Catechol	6600.82 ± 30.06
Resorcinol	6475.48 ± 193.28
Hydroquinone	1548.96 ± 135.79
Hydroxyquinol	2378.08 ± 153.28
Pyrogallol	4805.17 ± 206.72
Phloroglucinol*	3420.1 ± 87.4

*Ref: Chow, S.F., et al., Kinetic entrapment of a hidden curcumin cocrystal with phloroglucinol. Crystal Growth & Design, 2014. 14(10): p. 5079-5089.

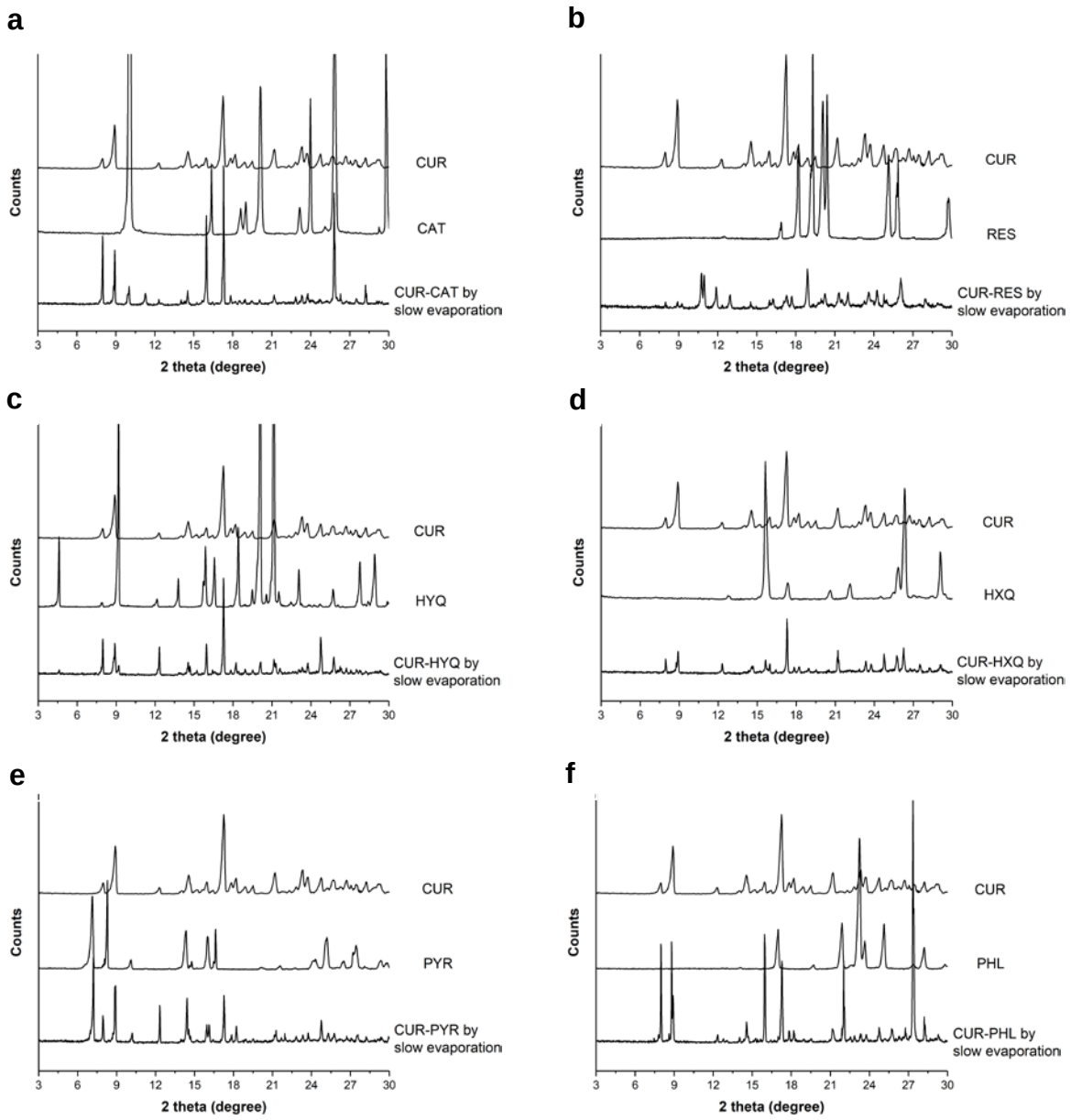

Figure S1. PXRD patterns of (a) CUR-CAT, (b) CUR-RES, (c) CUR-HYQ, (d) CUR-HXQ, (e) CUR-PYR, and (f) CUR-PHL cocrystal systems in a 1:1 stoichiometric ratio produced by slow evaporation in acetone.

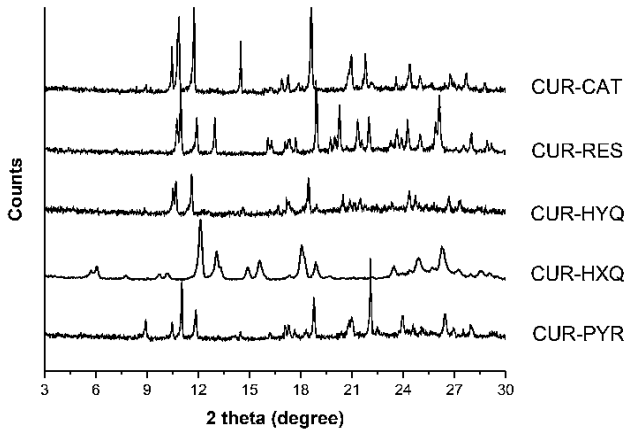

Figure S2. Overlaid PXRD patterns of CUR-CAT, CUR-RES, CUR-HYQ, CUR-HXQ and CUR-PYR cocrystals after 1 month of storage at 60 °C.

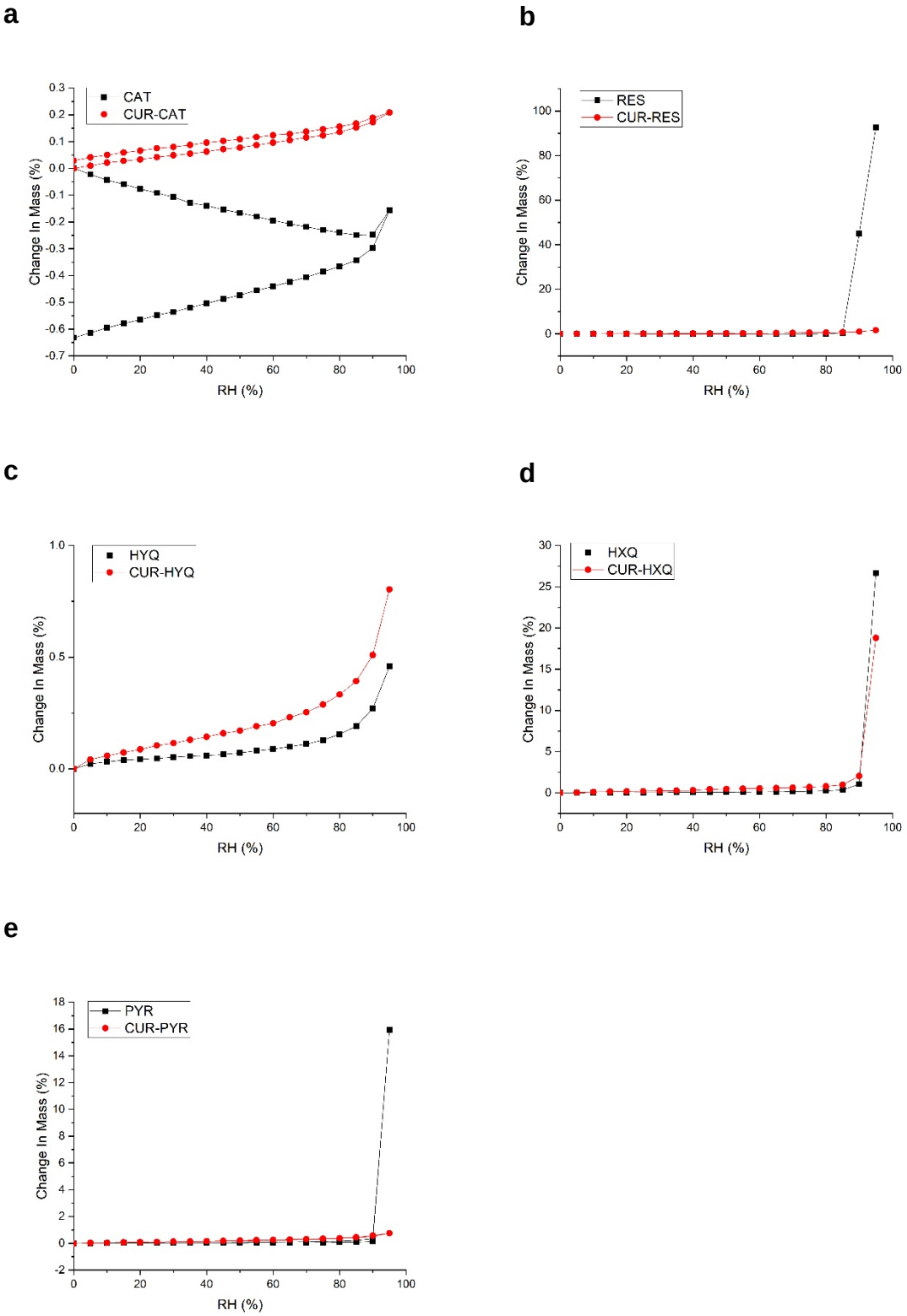

Figure S3. Moisture sorption isotherms of CUR cocrystals and the polyphenolic coformers.

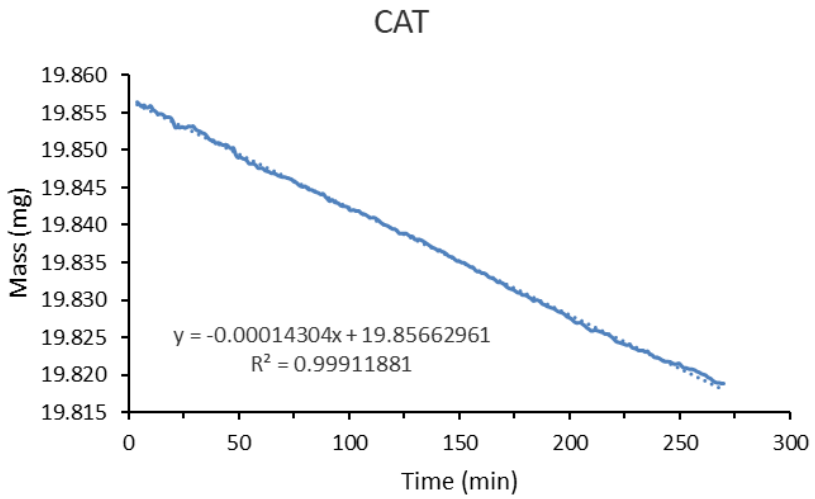

Figure S4. Weight loss curve of CAT, from which sublimation rate was calculated.

a

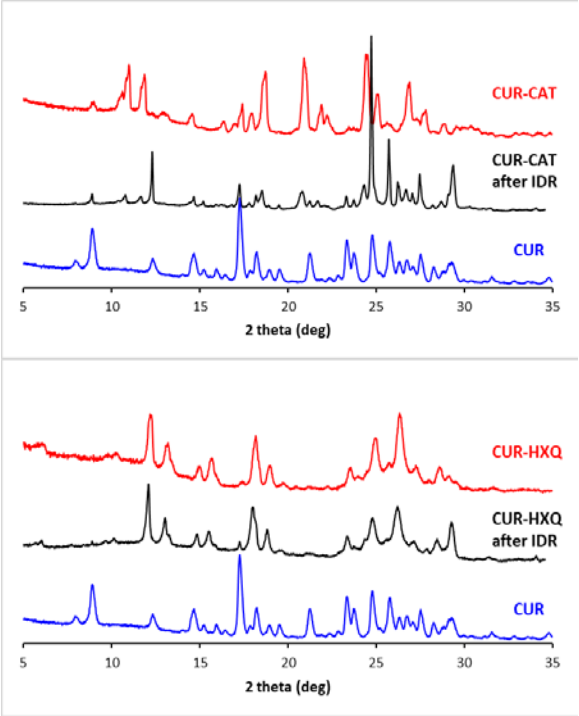

b

Figure S5. Phase transformation of CUR cocrystals during IDR experiments revealed by PXRD patterns a) fast phase transformation of CUR-CAT, b) slow phase transformation of CUR-HXQ.

a

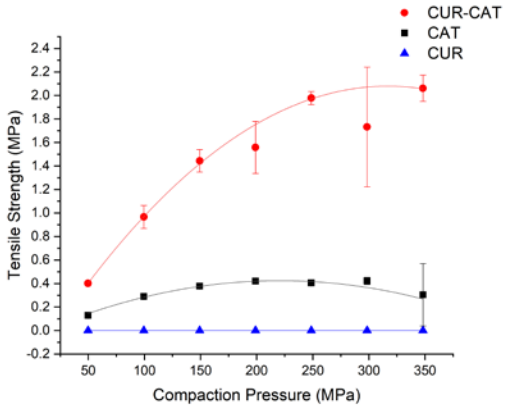
CUR-CAT
CAT
CUR
Tensile Strength (MPa)
Compaction Pressure (MPa)

b

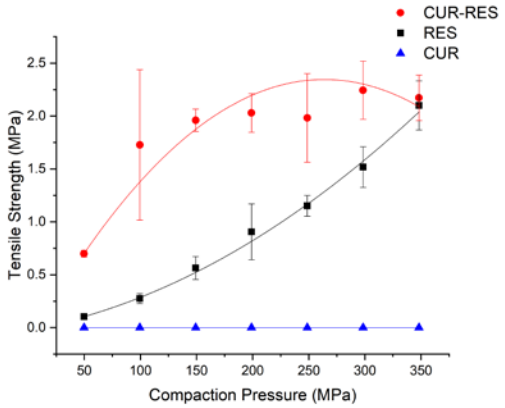
CUR-RES
RES
CUR
Tensile Strength (MPa)
Compaction Pressure (MPa)

c

d

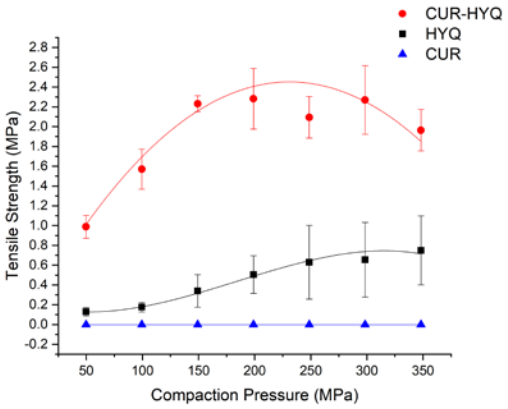

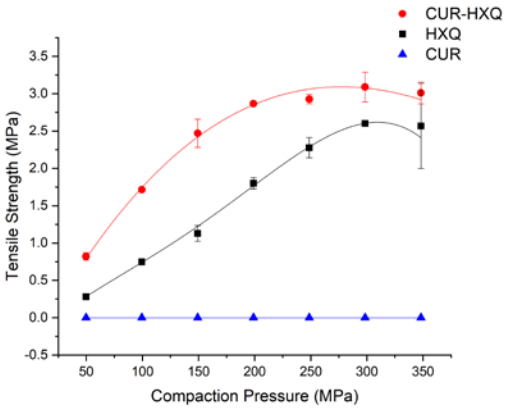

e

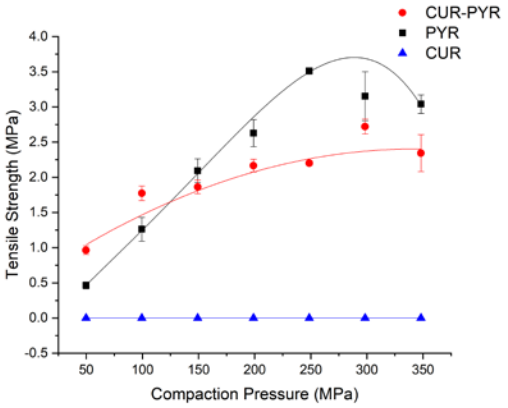

Figure S6. Tabletability of CUR, the polyphenolic coformers, and corresponding CUR cocrystals.